REMOTE SENS. ENVIRON. 50:303-316 (1994)

Retrieval of Surface Directional Reflectance Properties Using Ground Level Multiangle Measurements

*John V. Martonchik**

Knowledge of the directional reflectance properties of natural surfaces such as soils and vegetation canopies is essential for classification studies and canopy model inversion. Atmospheric correction schemes, using various levels of approximation, are described to retrieve surface bidirectional reflectance factors (BRFs) and directional-hemispherical reflectances (albedos) from multiangle radiance measurements taken at ground level. The retrieval schemes are tested on simulated data incorporating realistic surface BRFs and atmospheric models containing aerosols. Sensitivity of the atmospherically corrected BRFs and associated directional-hemispherical reflectances to various aerosol properties and the sun-view geometry is illustrated. A measurement strategy for obtaining highly accurate surface reflectance properties also is examined in the context of instrument radiometric calibration, knowledge of the atmospheric properties, and sun-view angular coverage.

INTRODUCTION

It is well known that natural surfaces do not behave as lambertian scatterers but exhibit anisotropic reflectance properties which depend on the characteristics of the surface. In general, the reflected radiance from a given surface type is a function of the solar zenith angle, the viewing zenith angle, and the difference between the solar and viewing azimuth angles. Measurements of directionally reflected radiation can be analyzed by means of physical surface models which provide information about the physical and optical properties of the surface (e.g., Pinty and Verstraete, 1991; 1992). The initial step in the analysis includes removing all effects of the atmosphere from the measurements (termed an atmospheric correction), resulting in surface bidirectional reflectances as produced by a beam of unattenuated direct sunlight. These reflectances then can be fitted to physical surface models typically through adjustment of a small number of parameters. Integration of these reflectances over the whole hemisphere of viewing angles defines the directional-hemispherical reflectance of the surface. The surface reflectance is an important parameter in a global sense because it is a factor in radiation balance studies, involving energy deposition, surface temperature, and evapotranspiration (Dickinson et al., 1990; Mintz, 1984; Charney et al., 1977).

Global, regional, and local area determinations of surface reflectance properties can only be accomplished effectively through the use of remote sensing platforms, either space-based or airborne. In particular the Multiangle Imaging SpectroRadiometer (MISR) (Diner et al., 1989) planned for launch in 1998 onboard NASA's Earth Observing System (EOS) AM-1 spacecraft and the airborne Advanced Solid-State Array Spectroradiometer (ASAS) (Irons et al., 1991) are both capable of making near simultaneous, downward-looking, multispectral, and multidirectional radiance measurements. It then is possible to determine land surface reflectance properties from this type of data through the use of suitable atmospheric correction algorithms (e.g., Martonchik and Diner, 1992; Martonchik et al., 1993; Markham et al., 1992). However, it is necessary that supplementary ground-based surface reflectance measurements be made at selected sites within the fields of view of these remote sensors so that the surface products derived from instruments like MISR or ASAS can be validated. Therefore, it is important that a correction procedure, termed

*Jet Propulsion Laboratory, Pasadena

Address correspondence to John V. Martonchik, Mail Stop 169-237, Jet Propulsion Laboratory, California Institute of Technology, 4800 Oak Grove Drive, Pasadena, CA 91109.

Received 24 November 1993; revised 25 June 1994.

0034-4257/94/$7.00

655 Avenue of the Americas, New York, NY 10010

a retrieval, also be performed on the ground-based reflectance measurements to remove any atmospheric effects and that it be as accurate as possible. This correction is required because diffuse sky radiance incident upon the surface produces a different angular distribution of the reflected radiance relative to what would be observed in the presence of only direct illumination.

In this article, results of a study are presented concerned with the surface reflectance retrieval process and some of the issues which can affect its accuracy. The accuracy issues fall into three basis categories: radiometric calibration of the sensor, knowledge of the atmospheric condition, and completeness of the angular geometry of the measurements. In this study radiometric calibration of the sensor and knowledge of the atmospheric condition initially are assumed to be perfect, and the focus is centered on the degradation of retrieval accuracy due to a limited range of angular geometry associated with the measurement set. In particular, simulated, ground level surface reflectance data sets are constructed utilizing a coupled surface–atmosphere radiative transfer code and including realistic surface bidirectional reflectance distribution functions and atmospheres with multiple scattering aerosols. These data sets, computed for selected view zenith angles, solar zenith angles, and relative azimuth angles, then are used in surface reflectance retrieval algorithms employing various degrees of approximation. The dependence of the retrieval accuracies of these various algorithms on atmospheric properties and sun position is investigated for a number of different trial cases. The issues of radiometric calibration and knowledge of the atmospheric properties and their effect on surface retrievals are then considered in some detail.

BACKGROUND

For a radiometrically calibrated instrument, the directionally reflected radiance L from a surface target, measured at ground level, can be written as

$$L(-\mu,\mu_0,\varphi-\varphi_\varphi) = \pi^{-1}\int_0^1\int_0^{2\pi} R(-\mu,\mu',\varphi-\varphi') \times L^{\text{inc}}(\mu',\mu_0,\varphi-\varphi_0)\mu'\,d\mu'\,d\varphi', \quad (1)$$

where $-\mu$ and μ_0 are the cosines of the view and solar zenith angles and $\varphi-\varphi_0$ is the view azimuthal angle with respect to the principal plane of the sun. The convention $-\mu$ and μ is used for upwelling and downwelling radiation, respectively. On the right-hand side of (1) L^{inc} is the total (direct and downward diffuse) radiance incident on the surface, and R is the bidirectional reflectance factor (BRF) of the surface target. The BRF of the surface target is defined as the bidirectional reflectance distribution function (BRDF) of the target ratioed to the BRDF of an ideal lambertian scattering surface (equal to $1/\pi$) (Nicodemus et al., 1977). It is assumed in this study that there is sufficient knowledge of the state of the atmosphere such that the atmosphere-dependent function L^{inc} in (1) either can be calculated to an arbitrary degree of accuracy or is measured directly. Then, given L at a number of different view angles, the problem is to retrieve R, the only unknown parameter, at the same view angles as L.

There are a number of instruments available which can measure directionally reflected radiation at the surface. One instrument in particular, the Portable Apparatus for Rapid Acquisition of Bidirectional Observations of the Land and Atmosphere (PARABOLA), has been used in a number of field studies (Deering and Leone, 1986). It is an automated, motorized radiometer that takes data in three wavelength bands (660 nm, 825 nm, and 1655 nm) and systematically makes measurements over both the downward and upward hemispheres with a 15° field-of-view. The PARABOLA data are usually expressed as experimental directional reflectance factors [or, more precisely, hemispherical-conical reflectance factors for nonisotropic incident radiation (Nicodemus et al., 1977)], obtained by ratioing the radiance within the instrument's field-of-view reflected from the surface target to a reference radiance measured at essentially the same time with the same instrument. This reference radiance usually is either the reflected radiance in the nadir direction from a calibrated near-lambertian (e.g., $BaSO_4$ or halon) reference panel or $1/\pi$ times the incident irradiance at the surface, a quantity derived from the upward-looking hemisphere measurements (downward diffuse radiance) and ancillary sun photometer data (direct solar irradiance).

Other instruments have been used in the field to measure directionally reflected radiation at the surface, but the angular coverage was usually restricted in comparison to PARABOLA. For example, Starks et al. (1991) used an MMR (Modular Multiband Radiometer) in the FIFE campaign to measure reflected radiation from prairie vegetation, but the view zenith angle range was limited to 50° on both sides of nadir, and the azimuth angle coverage was only in the principal plane of the sun. In this study only those measurement sets that exhibit relatively complete hemispherical coverage like PARABOLA are considered.

RETRIEVAL ALGORITHMS

The surface BRF retrieval algorithm described here makes use of an iteration approach which can accommodate the full hemispheric angular coverage of PARABOLA-like instruments. If the incident surface radiance L^{inc} is not measured and must be calculated, then it is assumed that the reflection properties of the terrain surrounding the target area are the same as the target

area to account adequately for the multiple reflections of radiation between the surface and the atmosphere in the algorithm. Thus, in that case reflectance measurements are assumed to be made on a fairly homogeneous surface region with sufficient horizontal extent.

Rigorous Approach

In the first step of the algorithm development, the radiance incident at the surface L^{inc} is separated into its direct and diffuse components, allowing (1) to be written as

$$L(-\mu,\mu_0,\varphi-\varphi_0) = \pi^{-1}R(-\mu,\mu_0,\varphi-\varphi_0) \times E_{dir}(\mu_0) + L_{diff}(-\mu,\mu_0,\varphi-\varphi_0). \quad (2)$$

Here E_{dir} is the direct incident irradiance at the surface and is assumed to be known, based, for example, on knowledge of the atmospheric optical depth obtained from associated sun photometry. L_{diff} is the upward diffuse radiance,

$$L_{diff}(-\mu,\mu_0,\varphi-\varphi_0) = \pi^{-1}\int_0^1\int_0^{2\pi} R(-\mu,\mu',\varphi-\varphi') \times L_{diff}^{inc}(\mu',\mu_0,\varphi'-\varphi_0)\mu'\,d\mu'\,d\varphi', \quad (3)$$

with L_{diff}^{inc} as the diffuse component of the incident radiance at the surface.

Using (2), the nth iteration of the retrieval algorithm for R then can be formally written as

$$R^{(n)}(-\mu,\mu_0,\varphi-\varphi_0) = \frac{L(\mu,\mu_0,\varphi-\varphi_0) - L_{diff}^{(n-1)}(-\mu,\mu_0,\varphi-\varphi_0)}{\pi^{-1}E_{dir}(\mu_0)}, \quad (4)$$

where $L_{diff}^{(n-1)}$ is computed using the $(n-1)$th iteration of R in (3). Various expressions for the initial estimate of the BRF, $R^{(0)}$, can be derived depending on the assumptions used. The simplest form assumes that the diffuse incident radiance is negligible compared to the direct incident radiance and that atmosphere–surface reflections can be ignored. Then, solving for R directly,

$$R^{(0)}(-\mu,\mu_0,\varphi-\varphi_0) = \frac{L(-\mu,\mu_0,\varphi-\varphi_0)}{\pi^{-1}E_{dir}(\mu_0)}. \quad (5)$$

For subsequent iterations L_{diff}^{inc} in (3) must be updated in addition to R, since the incident diffuse radiance normally includes multiple reflections between the surface and the atmosphere. Thus, for example, $L_{diff}^{(n-1)}$ in (4) is computed from (3) where L_{diff}^{inc} uses $R^{(n-1)}$ to describe the surface BRF.

Note that R, described by (4) or (5), is evaluated only at the reflectance (view) angles and incidence (sun) angle of the particular measurement set. To update L_{diff}, however, R must be evaluated over the complete range of the reflectance and incidence zenith angles and azimuth angles to perform the integrations as defined in (3). The updating of L_{diff}^{inc}, in particular, requires that R be evaluated at reflectance and incidence zenith angles defined for gaussian quadrature integration, necessary when accounting for the atmosphere–surface interaction. However, if the reflectance measurements L are made with an instrument like PARABOLA, the downward diffuse radiance L_{diff}^{inc} also is measured and can be directly inserted in (3), thus bypassing the process to compute it. Because of the hemispheric angular coverage of the measurements, the evaluation of R at the selected reflectance zenith angles and azimuth angles requires only the use of standard interpolation procedures. The evaluation of R over the full range of incidence zenith angle, however, can be accurately accomplished only if observations of a surface target are made at a number of different solar zenith angles. These multiple (distinct solar zenith angle) data sets then should be analyzed together so that the individual estimates of R at the different solar zenith angles using (4) or (5) can be introduced into (3) to compute L_{diff}, which then is used in (4) in the next iteration of the individual data sets. Depending on the number of sufficiently unique sun angle measurement sets, a linear or cubic spline technique generally is employed to interpolate or extrapolate the iterated estimates of R at the different solar zenith angles to gaussian quadrature incidence zenith angles for use in (3). If only a single sun angle measurement set is available, R is assumed to be independent of incidence zenith angle. The accuracy to which L_{diff} can be computed obviously depends on the accuracy to which the incidence zenith angle dependence of R can be estimated and thus directly affects the ultimate accuracy to which R can be retrieved.

Using (4) as expressed above, the iterated estimations of R generally tend to oscillate about the solution, normally resulting in a relatively slow convergence. The process can be made considerably more efficient simply by averaging the current iteration estimate of R from (4) with the previous iteration estimate. This modified current iteration estimate of R is substituted directly into (3) and also is used to update L_{diff}^{inc} to account more precisely for the atmosphere–surface multiple reflection process.

The directional hemispherical reflectance A of the surface is obtained by integrating the bidirectional reflectance factor over the projected view solid angle, that is,

$$A(\mu_0) = \pi^{-1}\int_0^1\int_0^{2\pi} R(-\mu,\mu_0,\varphi-\varphi_0)\mu\,d\mu\,d\varphi, \quad (6)$$

Since R is assumed to be retrieved over a sufficiently fine viewing angle grid in both zenith and azimuth angle, this integration can be performed using standard numerical procedures. The accuracy of A generally is limited by the retrieval accuracy of R and not the integration procedure.

Relaxed Approach

A distinctly faster and simpler but less accurate retrieval algorithm can be derived by relaxing the mathematical and physical rigor described in (3) and making some approximations. Starting from (2), the expression for reflected radiance can be rewritten as

$$L(-\mu,\mu_0,\varphi-\varphi_0)=\pi^{-1}R(-\mu,\mu_0,\varphi-\varphi_0)[E_{\mathrm{dir}}(\mu_0)+E''_{\mathrm{diff}}(\mu_0)]+\Delta(-\mu,\mu_0,\varphi-\varphi_0) \quad (7)$$

where E''_{diff} is the incident diffuse irradiance including all multiple reflections between the surface and atmosphere, and Δ is a residual term,

$$\begin{aligned}\Delta(-\mu,\mu_0,\varphi-\varphi_0)=\pi^{-1}&\int_0^1\int_0^{2\pi}R(-\mu,\mu',\varphi-\varphi')\\&\times L^{\mathrm{inc}}_{\mathrm{diff}}(\mu',\mu_0,\varphi'-\varphi_0)\mu'\,d\mu'\,d\varphi'\\&-\pi^{-1}R(-\mu,\mu_0,\varphi-\varphi_0)\\&\times\int_0^1\int_0^{2\pi}L^{\mathrm{inc}}_{\mathrm{diff}}(\mu',\mu_0,\varphi'-\varphi_0)\\&\times\mu'\,d\mu'\,d\varphi'. \quad (8)\end{aligned}$$

Note that the integral in the last term in (8) is equal to E''_{diff}. The residual Δ can be small depending on the characteristics of R (little dependence on incidence and azimuth angles) or the amount of atmospheric optical depth (small $L^{\mathrm{inc}}_{\mathrm{diff}}$). Now, if it is assumed that the surface behaves as a lambertian scatterer when considering multiple reflections between the surface and the atmosphere, then the total incident irradiance at the surface can be written as

$$\begin{aligned}E_{\mathrm{dir}}(\mu_0)+E''_{\mathrm{diff}}(\mu_0)&=\frac{E_{\mathrm{dir}}(\mu_0)+E_{\mathrm{diff}}(\mu_0)}{1-A(\mu_0)\cdot S}\\&=E_{\mathrm{dir}}(\mu_0)+\frac{A(\mu_0)\cdot S\cdot E_{\mathrm{dir}}(\mu_0)}{1-A(\mu_0)\cdot S}\\&\quad+\frac{E_{\mathrm{diff}}(\mu_0)}{1-A(\mu_0)\cdot S}. \quad (9)\end{aligned}$$

E_{diff} is the incident diffuse irradiance, assuming no atmosphere-surface interaction (i.e., a black surface), A is the directional-hemispherical reflectance of the surface, and S is defined by

$$\begin{aligned}S=\pi^{-1}&\int_0^1\int_0^{2\pi}\int_0^1\int_0^{2\pi}s(\mu',-\mu'',\varphi'-\varphi'')\\&\times\mu'\,d\mu''\,d\varphi''\,d\mu'\,d\varphi', \quad (10)\end{aligned}$$

with s representing the atmospheric reflectance function for radiation scattered from the underside of the atmosphere. Like E_{dir}, both E_{diff} and S are computed, assuming knowledge of the atmospheric properties. Note that both the direct irradiance and the black surface diffuse irradiance terms on the right-hand side of (9) must be divided by the factor $(1-AS)$ to account fully for the multiple reflections of radiation between the surface and atmosphere.

Using (7) and (9), the surface BRF then can be expressed as

$$R(-\mu,\mu_0,\varphi-\varphi_0)=\frac{[L(-\mu,\mu_0,\varphi-\varphi_0)-\Delta(-\mu,\mu_0,\varphi-\varphi_0)]}{\pi^{-1}[E_{\mathrm{dir}}(\mu_0)+E''_{\mathrm{diff}}(\mu_0)]} \quad (11)$$

$$\cong\frac{L(-\mu,\mu_0,\varphi-\varphi_0)[1-A(\mu_0)\cdot S]}{\pi^{-1}[E_{\mathrm{dir}}(\mu_0)+E_{\mathrm{diff}}(\mu_0)]} \quad (12)$$

when Δ is assumed small and is ignored. Expression (12) is similar to the estimate of R described by (5) but includes the contibution of E_{diff} and an approximation for the multiple reflections of radiation between the surface and atmosphere. Integrating (12) in accordance with (6), the hemispherical-directional reflectance A is given by

$$A(\mu_0)=\frac{G(\mu_0)}{1+G(\mu_0)\cdot S}, \quad (13)$$

where

$$\begin{aligned}G(\mu_0)=&\frac{1}{[E_{\mathrm{dir}}(\mu_0)+E_{\mathrm{diff}}(\mu_0)]}\\&\times\int_0^1\int_0^{2\pi}L(-\mu,\mu_0,\varphi-\varphi_0)\mu\,d\mu\,d\varphi. \quad (14)\end{aligned}$$

G is the ratio of irradiance leaving the surface to the incident (black surface) irradiance and is calculated directly from the measurements L and the model atmosphere values of E_{dir} and E_{diff}. Then A can be calculated from (13) using the model atmosphere value for S, followed by an evaluation of R by means of (12). This retrieval scheme for R is one to two orders of magnitude faster than the more rigorous, iterative version described previously. Since this relaxed, noniterative version does not include any incidence angle dependence of R (such dependence being contained solely in the neglected parameter Δ), it generally will be less accurate than the rigorous version.

The above expressions for the relaxed version of the retrieval algorithm assumed that the incident diffuse radiance $L^{\mathrm{inc}}_{\mathrm{diff}}$ was not measured. If this is not the case, then the surface BRF can be obtained directly from (7),

$$R(-\mu,\mu_0,\varphi-\varphi_0)=\frac{[L(-\mu,\mu_0,\varphi-\varphi_0)-\Delta(-\mu,\mu_0,\varphi-\varphi_0)]}{\pi^{-1}[E_{\mathrm{dir}}(\mu_0)+E''_{\mathrm{diff}}(\mu_0)]} \quad (11)$$

$$\cong\frac{L(-\mu,\mu_0,\varphi-\varphi_0)}{\pi^{-1}[E_{\mathrm{dir}}(\mu_0)+E''_{\mathrm{diff}}(\mu_0)]} \quad (15)$$

where E''_{diff} is computed by integrating the directional incident diffuse radiance measurements, that is,

$$E''_{\mathrm{diff}}(\mu_0)=\int_0^1\int_0^{2\pi}L^{\mathrm{inc}}_{\mathrm{diff}}(\mu',\mu_0,\varphi'-\varphi_0)\mu'\,d\mu'\,d\varphi'. \quad (16)$$

Ratioing Approach

It is informative to compare R in (12) or (15) with the expression for the experimental directional reflectance factor, described earlier as the ratio of directionally reflected radiance from the surface target to the nadir radiance from a reference target. Assuming that the reference target is ideally lambertian, the reflected radiance from the reference target can be expressed by (7), rewritten as

$$L_{\text{ref}}(\mu_0) = \pi^{-1}[E_{\text{dir}}(\mu_0) + E''_{\text{diff}}(\mu_0)], \tag{17}$$

where the BRF, R, is by definition unity for an ideal lambertian surface and Δ is zero. Using (11), the ratioed radiances of the surface target to the reference target then is

$$\begin{aligned}\frac{L(-\mu,\mu_0,\varphi-\varphi_0)}{L_{\text{ref}}(\mu_0)} &= \frac{L(-\mu,\mu_0,\varphi-\varphi_0)}{\pi^{-1}[E_{\text{dir}}(\mu_0) + E''_{\text{diff}}(\mu_0)]} \\ &= R(-\mu,\mu_0,\varphi-\varphi_0) \\ &\quad + \frac{\pi\Delta(-\mu,\mu_0,\varphi-\varphi_0)}{[E_{\text{dir}}(\mu_0) + E''_{\text{diff}}(\mu_0)]}.\end{aligned} \tag{18}$$

Note that (18) is almost the same expression as (12) or (15) and therefore essentially describes the relaxed algorithm when Δ is assumed to be negligible. If Δ is indeed negligible, interpreting the ratioed surface reflectance measurements as bidirectional reflectance factors results in a valid correction for atmospheric effects. Field measurements by Deering and Eck (1987), however, can show that Δ can be quite substantial under hazy conditions, thereby reducing the accuracy of the determination of R by the ratioing technique.

It should be noted that a conceptual difference exists between (12) and (18) because the reflection properties of the surface are considered to be lambertian in the atmosphere–surface multiple reflection process describing the incident radiance in (12) whereas the true total incident radiance is used in (18). A comparison of computational results between the two situations, however, showed only insignificant differences for the various atmospheric conditions and surface types considered in this study, indicating that a high degree of accuracy still is retained when using the lambertian approximation. Expression (15) is virtually identical to (18) and the only difference between them is that E_{dir} is directly measured as part of L_{ref} in (18) whereas it is determined by ancillary measurements (e.g., sun photometry) in (12) and (15). Thus, both (12) and (15) can be used as an equivalent representation of (18) and use of the relaxed version of the retrieval algorithm can be considered to be equivalent to the ratioing procedure.

MULTIANGLE RADIANCE DATA SETS

The rigorous and relaxed surface reflectance retrieval algorithms were applied to various sets of simulated multiangle radiances, computed for different types of directionally reflecting surfaces overlain by an atmosphere containing aerosols. The bidirectional reflectance factors describing the surface reflection properties were derived from measurements, made under clear skies, of 11 distinct types of natural surfaces in AVHRR wavelength Bands 1 and 2 at 0.58–0.67 μm and 0.73–1.1 μm, respectively (Kimes, 1983; Kimes et al., 1985a,b). Thus, these measurements provided 22 distinct BRF cases to be analyzed in this study. The characteristics of the various surface types are listed in Table 1. These experimental reflectance factors, obtained by the ratioing technique, are not the actual bidirectional reflectance factors of the surface because of the potential impact of the Δ term effect discussed above and because of angular smoothing effects due to the finite (12°) field-of-view of the instrument. For the purposes of this study, however, it was assumed that the experimental reflection factors are the true surface bidirectional reflectance factors.

The measurements were made over the entire azimuth angle range, starting from the principal plane and proceeding in 45° increments, and over the zenith angle range from 0° to 75° in 15° increments for a total of 41 unique measurements per solar zenith angle. To guarantee reflection symmetry through the principal plane, the mirror-image radiance pairs through the principal plane were averaged, thus leaving a total of 26 independent data points per measurement set. The solar zenith angle coverage varied, depending on the surface type, but measurements were usually made at three or four different sun positions. Solar zenith angle coverage for the complete set of 11 surface types ranged between 23° and 82°. A two-dimensional cubic spline interpolation scheme then was applied to these data sets to compute the BRF at arbitrary incidence and reflection angles for use in the radiative transfer procedure.

Three different sun geometries were investigated, defined by solar zenith angles of 25.6°, 45.9°, and 64.0° and an azimuth angle φ_0 of 0°. The directional hemispherical reflectances for the 11 surface types in the two spectral bands and at the three selected sun angles were computed by integrating the BRF over view angle according to (6) and are displayed in the bar graphs shown in Figures 1a and 1b. They range from a low of 0.032 (soybeans, case 10 in Band 1 at a sun angle of 45.9°) to a high of 0.621 (irrigated wheat, case 5 in Band 2 at a sun angle of 64.0°). The corresponding BRF cases also have a wide variety of shapes, ranging from strong backward and forward scattering to little or no angular variability. For example, soil (Case 1) exhibits strong backward scattering in Band 1 which is highly dependent on sun angle, while a pine forest (Case 7) exhibits moderate forward and backward scattering in Band 1 for most sun angles. These two surface types represent the reflection variability extremes for the

Table 1. Surface Type Characteristics

Case	*Cover Type*	*Location*	*Height (cm)*	*Coverage (%)*
1	Plowed field	Tunisia, Africa	–	–
2	Grassland	Tunisia, Africa	<3	<5
3	Steppe grass	Tunisia, Africa	38	18
4	Hard wheat	Tunisia, Africa	46	11
5	Irrigated wheat	Tunisia, Africa	76	70
6	Hardwood forest	Beltsville, Maryland	1100	75
7	Pine forest	Beltsville, Maryland	2200	79
8	Lawn grass	Beltsville, Maryland	14	97
9	Corn	Beltsville, Maryland	33	25
10	Soybeans	Beltsville, Maryland	77	90
11	Orchard grass	Beltsville, Maryland	22	50

cases in Table 1 and are used as examples in the subsequent retrieval analysis.

The atmospheric models used in the radiance simulations contain both Rayleigh and aerosol scattering. The Rayleigh optical depth was set to 0.049 for Band 1 and 0.010 for Band 2 with a standard atmospheric scale height. The optical properties of the aerosols were assumed to be identical in Bands 1 and 2. The aerosol scattering was assumed to be Mie with a phase function described by an asymmetry parameter g of 0.517, a single-scattering albedo ω of 1.0, and with a particle density scale height of 2 km. A number of different aerosol optical depths τ were considered, ranging from 0.0 to 0.5.

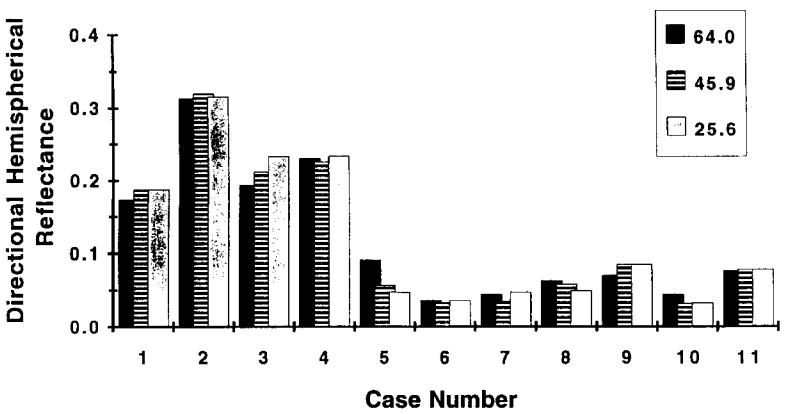

(a)

Figure 1a. Histogram of directional hemispherical reflectance (albedo) in Band 1 for the surface BRF cases listed in Table 1. The reflectances for three different solar zenith angles are displayed for each case.

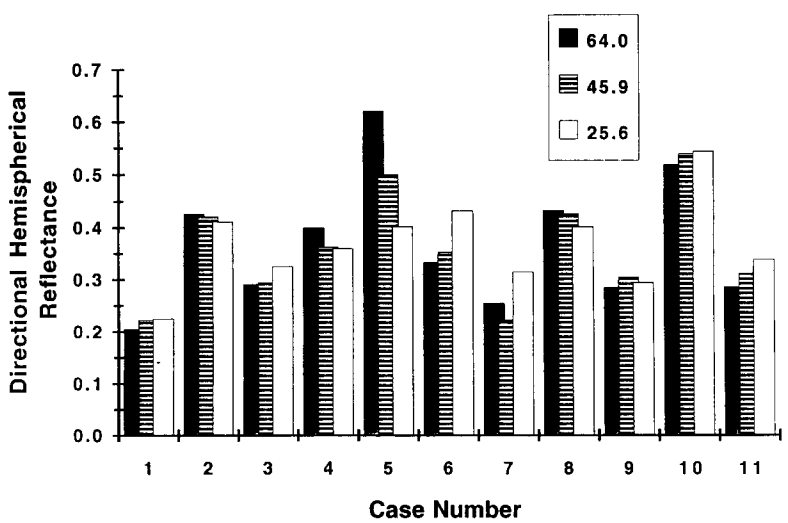

(b)

Figure 1b. Same as Figure 1a except reflectances are for Band 2.

Using the 22 surface BRF cases and the aerosol-laden atmospheric models described above, simulated ground-level radiance data sets for a PARABOLA-like instrument were computed using a coupled atmosphere–surface radiative transfer code (Grant and Hunt, 1968) with view angles set at the same values as the experimental directional reflectances noted above. As a simplification, the simulated data sets do not include the effects of a finite view solid angle. If the retrieval is to be performed on a real data set, however, it is straightforward to include an integration over the view solid angle in the described retrieval algorithms.

RETRIEVAL RESULTS

In this part of the retrieval study we first test the accuracy of the iterative retrieval scheme described by expressions (3), (4), and (5). To achieve maximum accuracy in the retrieval process, a combined data set was used which included the reflection measurements at all three of the noted solar zenith angles (25.6°, 45.9°, and 64.0°). Use of the three sun angle sets together instead of individually allows a more accurate computation of L_{diff} as expressed by (3) since the sun angle dependence of R and $L_{\text{diff}}^{\text{inc}}$ more readily can be taken into account. For the heavily laden aerosol condition ($\tau = 0.5$), the retrieval bidirectional reflectance factors for the 11 BRF cases in Band 1 are displayed in Figure 2, expressed in terms of the fractional deviation δ, for each sun position. The fractional deviation δ for a given BRF type is defined as

$$\delta(\mu_0) = \frac{1}{N}\sum_{ij} \left| \frac{R(\mu_i,\mu_0,\varphi_j-\varphi_0) - R_0(\mu_i,\mu_0,\varphi_j-\varphi_0)}{A(\mu_0)} \right|, \qquad (19)$$

where R and R_0 are the retrieved and true bidirectional reflectance factors, respectively, A is the true directional hemispherical albedo, and N is the number of unique measurements (26 for the described data sets) at the given sun position. A is used in the denominator of (19) instead of R_0 so as to not unduly weight extremely small values of R_0. Similar results to those of Band 1 were obtained for the BRF cases of Band 2, as was true for all aspects of this study. Therefore, in the interest of brevity, only the results from Band 1 are illustrated in this article.

Although the irrigated wheat BRF (Case 5) at 64.0° solar zenith angle in Band 1 shows a fractional deviation as high as 0.096, the average fractional deviation for the 22 BRF cases is under 0.03. Research into the cause of the much larger than average deviations associated with Cases 1, 5, 6, and 7 in Figure 2 showed that the BRF variation with incidence angle for these cases was strong and the three sun angle data sets used in the retrievals were not sufficient in number to totally account for such a wide range of variation. Note also that from (19) the average error in the retrieved BRF is given by the product of $\delta(\mu_0)$ and $A(\mu_0)$. Thus, for example, for Case 5 at 64.0° solar zenith angle the average BRF error is only $0.096 \times 0.090 = 0.0086$.

The directional hemispherical reflectances computed from the retrieved bidirectional reflectance factors for the 11 cases in Band 1 are shown in Figure 3 as a percent difference from the correct values of Figure 1 (i.e., 100% × (retrieved − true) / true). The largest errors in the hemispherical reflectances reach about 8%, but the average error for all 22 BRF cases is just over 2%. Retrievals were also done on the data sets where the aerosol loading was not so great and the results show the same trends as the heavy loading situation but with a steady improvement in accuracy with decreasing aerosol optical depth. For the data sets with an optical depth of 0.1 there is about a factor of 2 improvement in retrieval accuracy over those data sets with an optical depth of 0.5, for both the individual BRF cases and the directional hemispherical reflectances.

To determine how sensitive the retrieval results are

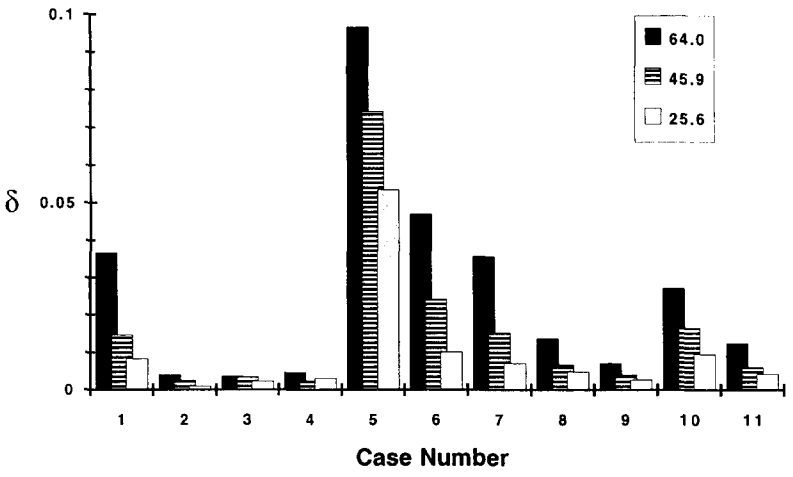

Figure 2. Retrieval of BRF in Band 1 expressed as average fractional deviation (see text) using the rigorous algorithm and the combined reflectance data sets at the three solar zenith angles.

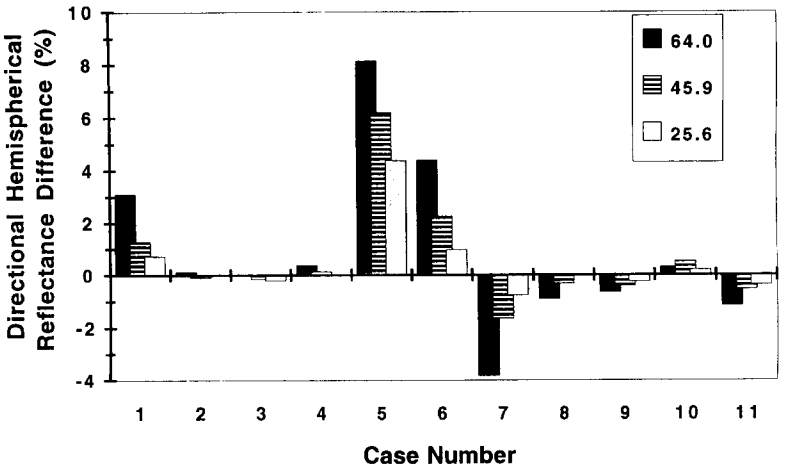

Figure 3. Percent difference in directional hemispherical reflectances in Band 1 computed from retrieved bidirectional reflectance factors using the rigorous algorithm.

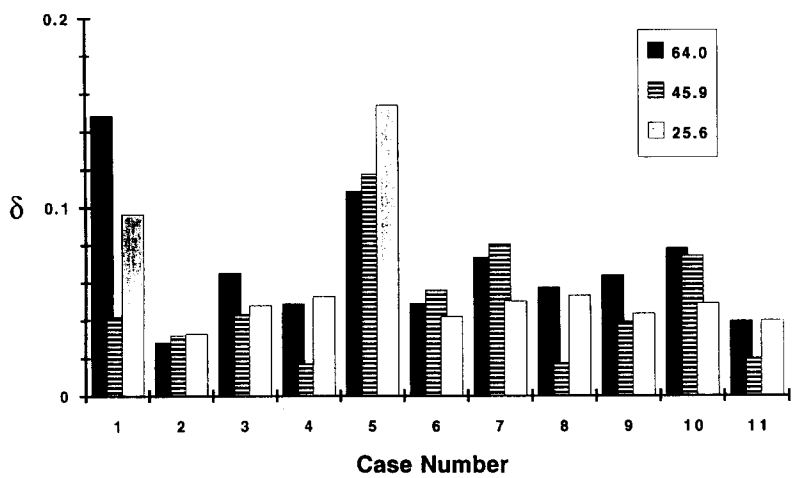

Figure 4. Retrieval of BRF in Band 1 using the intermediate algorithm independently on each of the reflectance data sets at the three solar zenith angles.

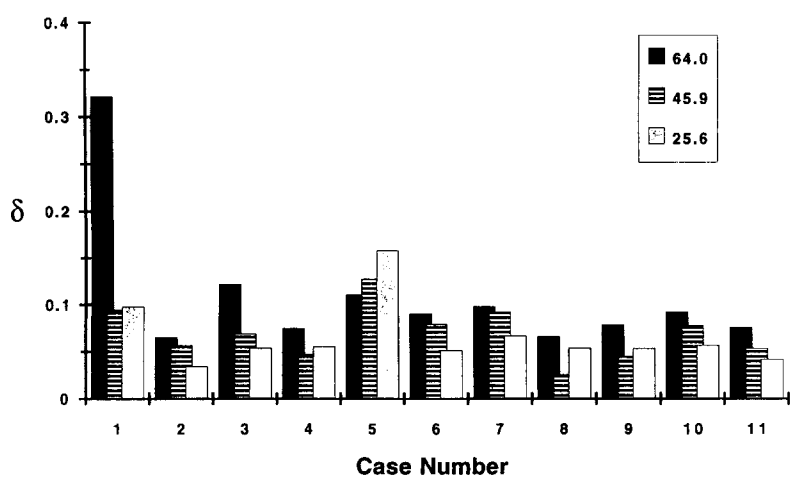

Figure 5. Retrieval of BRF in Band 1 using the relaxed, noniterative algorithm independently on each of the reflectance data sets at the three solar zenith angles.

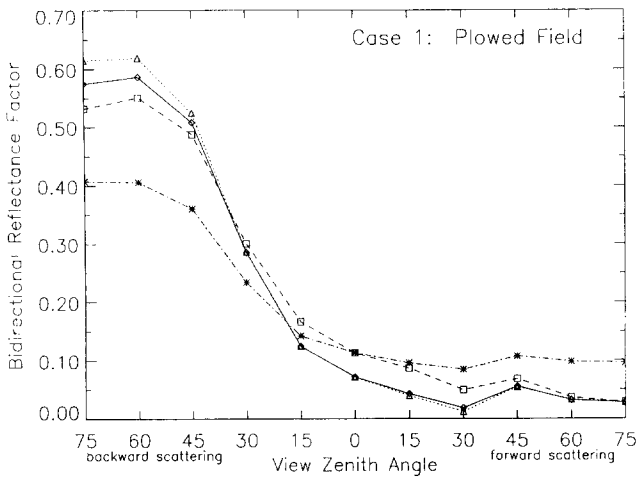

Figure 6. Retrieved BRF in Band 1 in the principal plane for case 1 (plowed field) using the rigorous (triangles), intermediate (squares), and relaxed (stars) algorithms. For comparison the correct BRF is also shown (diamonds).

to sun angle coverage of the measurements, retrievals were performed on the same data sets as above but used only a single sun angle data set per retrieval trial. Thus, three independent trials were run at each of the specified sun angles. This method implies that the μ' dependence in the integral of (3) is replaced by the constant μ_0 of the particular sun geometry being considered in the retrieval process, but that the azimuthal angle dependence $\varphi - \varphi'$ for that sun geometry is still maintained within the integral. This is, therefore, an intermediate case between that of the rigorous retrieval algorithm which considers the full μ', $\varphi - \varphi'$ dependence of R by using multiangle sun geometry data sets and the relaxed algorithm which replaces the $\mu', \varphi - \varphi'$ dependence with the particular μ_0, $\varphi - \varphi_0$ of a single-angle sun geometry data set. Figure 4 shows the retrieval results in Band 1, expressed as fractional deviations, using this intermediate retrieval algorithm on those data sets produced with an aerosol optical depth of 0.5. The corresponding results for the same data sets but using the relaxed algorithm described by (12) are displayed in Figure 5. Sample comparisons in accuracy between the various algorithms of the retrieved bidirectional reflectance factors in the principal plane are illustrated in Figures 6, 7, and 8 for the individual cases of the plowed field, irrigated wheat, and the pine forest, respectively, at a solar zenith angle of 64.0°. A significant reduction in accuracy is evident when the results from either of these two alternative algorithms are compared to those from the rigorous algorithm. This accuracy degradation also applies to the retrieved directional hemispherical reflectances, displayed in Figures 9 and 10, when using either the intermediate or relaxed algorithm. For those data sets produced with progressively smaller aerosol optical depths, the retrieval results followed the same trends as those illustrated for the data sets with an optical depth of 0.5 but with systematically increasing accuracy. The retrieval results for the data sets with an aerosol optical depth of 0.1, for example, were three to four times more accurate than the results in Figures 5–10.

From these trials it can be concluded that retrievals using combined multiangle sun geometry data sets produce results with greater accuracy than retrievals using only a single sun angle data set. In turn, when a single sun angle data set is processed, the intermediate retrieval algorithm generally is more accurate than the relaxed algorithm. These conclusions are particularly true for those BRF cases which have a strong dependence on both solar zenith angle and solar azimuth angle, a good example being that of soil as displayed in Figure 6. When the solar angle dependence is less extreme, as in the case of the pine forest BRF case shown in Figure 8, which, nevertheless, has a significant

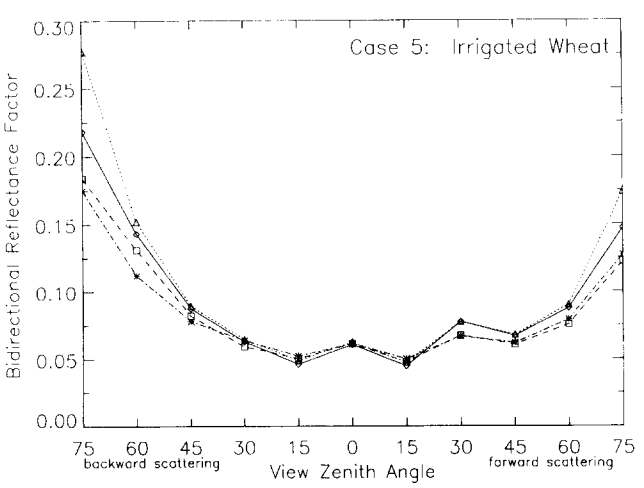

Figure 7. Same as Figure 6 but for Case 5 (irrigated wheat).

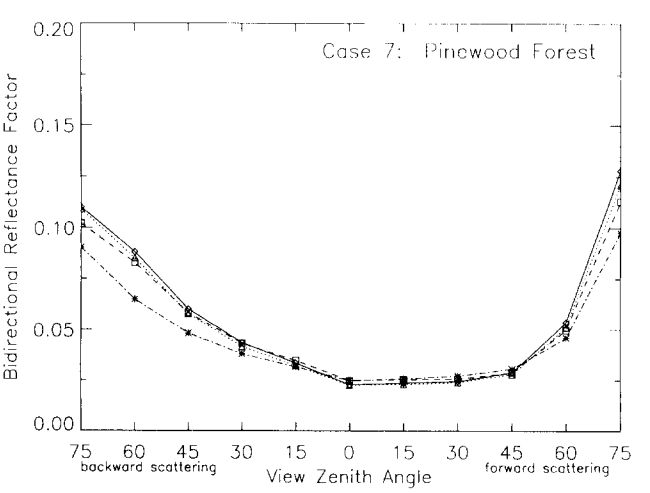

Figure 8. Same as Figure 6 but for Case 7 (pine forest).

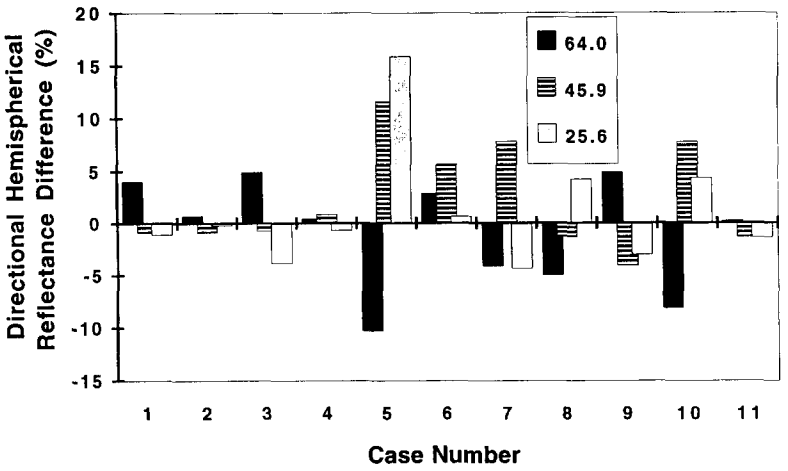

Figure 9. Percent difference in directional hemispherical reflectances in Band 1 computed from retrieved bidirectional reflectance factors using the intermediate algorithm.

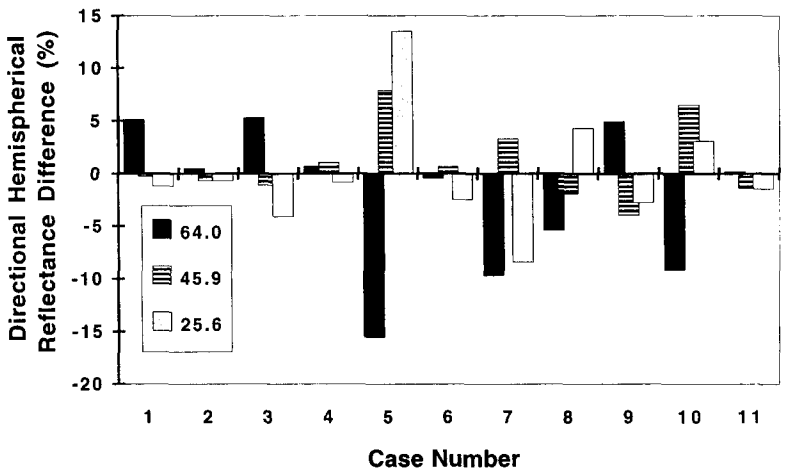

Figure 10. Percent difference in directional hemispherical reflectances in Band 1 computed from retrieved bidirectional reflectance factors using the relaxed algorithm.

view angle dependence, the retrieval results from the various algorithm versions described here tend to be more similar to each other.

The trials also showed that the amount of atmospheric optical depth can strongly influence the accuracy of the retrieval results, depending on the version of the algorithm used. Figure 11 shows a summary of the retrieval tests for both the rigorous and relaxed algorithms, illustrating the dependence of the case-averaged (22 BRF cases of Bands 1 and 2) fractional deviation δ on the amount of aerosol optical depth. The corresponding results from the intermediate algorithm are not shown to avoid clutter but they tend to fall in the gap between those from the other two algorithms. For no aerosol the case-averaged δ is about 0.003, due to computational errors accrued during the removal of the effects of the Rayleigh optical depth. When the aerosol optical depth is on the order of 0.1 or less, both the rigorous and intermediate algorithms have essentially the same accuracy and the relaxed algorithm only a little less accuracy. Thus, the ratioing procedure, applied to field measurements taken under light aerosol loading (in effect, an application of the relaxed algorithm), results in atmospherically corrected experimental reflectance factors which are reasonable representations of the true surface bidirectional reflectance factors. For those measurements, however, made when the atmospheric optical depth is substantial (0.3 and greater), the accuracy of the atmospheric correction process can be severely compromised if the ratioing technique is employed. Under these conditions the intermediate algorithm should be used if the measurement set includes only one sun angle. When measurements at more than one sun angle are available, the more rigorous iterative retrieval algorithm is preferred.

It should be emphasized that multiangle sun geometry data sets can generally have different aerosol conditions associated with each sun angle set. This may occur because the aerosol amount changed during the course of a day's worth of measurements or else data sets from different days are combined. This presents no problem to the use of the rigorous algorithm since each particular sun angle data subset of the combined data set is processed using either an atmospheric model appropriate

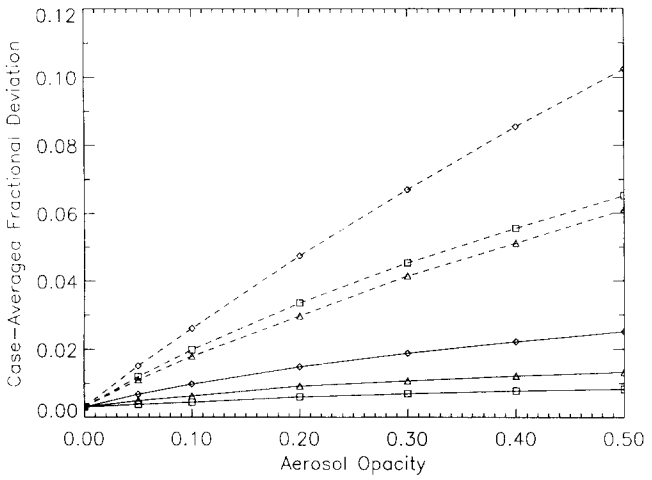

Figure 11. Retrieved BRF fractional deviation, averaged over the 22 cases, as a function of aerosol optical depth. Both the rigorous (solid lines) and relaxed algorithm (dashed lines) results are shown for the three solar zenith angles (64.0°, diamonds; 45.9°, triangles; 25.6°, squares).

for the atmospheric conditions when the measurements were taken or else using the actual measurements of the downward diffuse radiance.

DISCUSSION

The retrieval trials described above show that BRF accuracies with a δ of 0.03 or better can be achieved when all other factors are strictly controlled. In particular it was assumed that the atmospheric conditions were precisely known and therefore did not compromise the accuracy of the retrieval results. If ancillary atmospheric measurements are taken in the same time period as the surface reflectance measurements, however, they typically include only sun photometry to determine the spectral aerosol optical depth. Generally no other kinds of measurements are made from which to obtain additional aerosol information such as spectral single scattering albedos and phase functions.

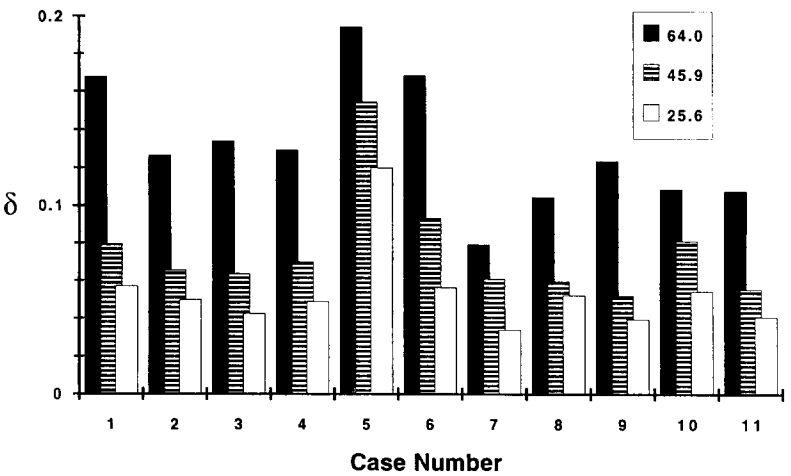

Figure 12. Retrieval of BRF in Band 1 using the rigorous algorithm, the combined reflectance data sets at the three solar zenith angles, and a modified aerosol model in which $\omega = 0.9$ instead of 1.0.

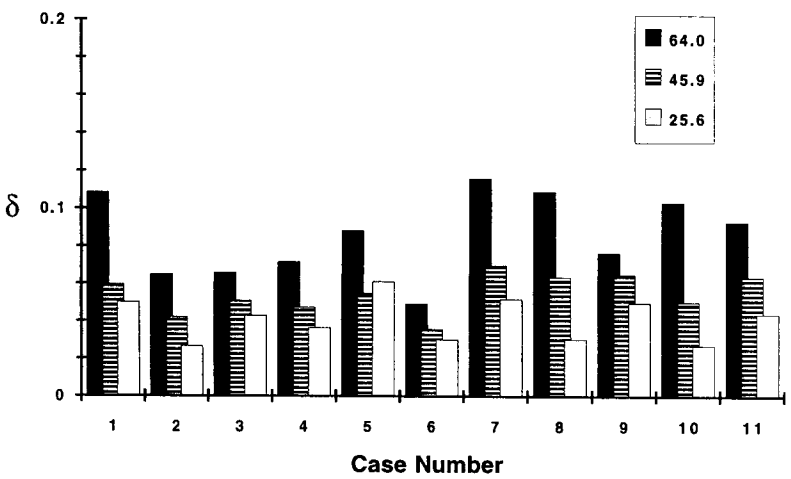

Figure 13. Retrieval of BRF in Band 1 using the rigorous algorithm, the combined reflectance data sets at the three solar zenith angles, and a modified aerosol model in which $g = 0.714$ instead of 0.517.

The impact of uncertainties in the atmospheric parameters on surface BRF retrieval is illustrated in Figures 12 and 13. Figure 12 shows the fractional deviation δ assuming the same retrieval conditions as those that produced Figure 2 except that an aerosol single scattering albedo ω of 0.9 was used instead of 1.0. Note the strong, systematic solar zenith angle dependence of δ, averaging more than 0.13 at 64.0° and receding to less than 0.06 at 25.6°. The corresponding directional hemispherical reflectances show a similar trend with an average percent increase of more than 11% at solar zenith angle of 64.0° and about 5% at 25.6°. Figure 13 shows a similar trend when, again, the correct atmospheric conditions were assumed in the retrieval except that a stronger forward scattering aerosol phase function was used (asymmetry parameter g of 0.714 instead of 0.517). Again, the increase in δ with solar zenith angle is evident, the average ranging from about 0.08 at 64.0° down to about 0.04 at 25.6°. The corresponding directional hemispherical reflectances are systematically smaller than the correct values with the average percent difference being about −9% at solar zenith angle of 64.0° and about −3% at 25.6°.

A useful field data set which can help validate the aerosol model used in the surface retrieval is measurements of the incident (downward) diffuse sky radiance in a number of different directions. The value of an instrument like PARABOLA is its ability to measure diffuse sky radiance over most of the upward-looking hemisphere during the course of measuring the surface reflected radiance. When a subsequent surface retrieval is done using a particular aerosol model, it is straightforward to compute the associated downward radiances to which the measured sky radiance values can be compared. Figure 14 shows such a comparison of downward diffuse radiance in the principal plane for the three aerosol models previously considered, namely the correct model ($\omega = 1.0$, $g = 0.517$), and its two variations ($\omega = 0.9$, $g = 0.517$) and ($\omega = 1.0$, $g = 0.714$), all with an aerosol optical depth of 0.5. The radiances for surface BRF Case 1 (plowed field) at solar zenith angle 25.6° is illustrated, but similar radiances at the same solar zenith angle are obtained for the other surface types. It is clear that the differences in the downward diffuse radiance predicted for the two variant aerosol models from that of the correct model directly account for the increased BRF retrieval deviations of Figures 12 and 13 as compared to Figure 2. This problem of needing to know the atmospheric properties as a necessary condition for accurate surface reflectance retrievals can be completely bypassed, however, by making use of the measured incident diffuse radiances directly in the rigorous retrieval algorithm, as described earlier.

The other major factor affecting the accuracy of the surface retrieval is the quality of the radiometric calibration of the instrument. Even if both the upward reflected surface radiance L and the incident diffuse radiance $L_{\text{diff}}^{\text{inc}}$ are simultaneously measured by the same instrument, it can be seen from expressions (4), (12), and (15) that the bidirectional reflectance factors, retrieved by either the rigorous or relaxed forms of the algorithm, are directly affected by errors in the radiometric calibration. This is due to the fact that the direct irradiance E_{dir} is normally determined by means of another instrument such as a sun photometer. However, the ratioing technique, described by expression (18), is completely insensitive to any radiometric calibration errors because both the direct and diffuse radiance are effectively measured by the same instrument by means of the reference target. Rewriting (18),

$$R(-\mu,\mu_0,\varphi-\varphi_0) = \frac{L(-\mu,\mu_0,\varphi-\varphi_0)-\Delta(-\mu,\mu_0,\varphi-\varphi_0)}{L_{\text{ref}}(\mu_0)}, \tag{20}$$

a general form for R with no approximations. When incident diffuse radiance measurements $L_{\text{diff}}^{\text{inc}}$ are also made in addition to L and L_{ref}, then Δ, described by (8), has the same calibration accuracy as L and L_{ref} and the evaluation of R via (20) will be insensitive to calibration errors. If the reference target is only approximately an ideal lambertian reflector, L_{ref} in (20) can be replaced by L''_{ref}, where

$$\begin{aligned} L''_{\text{ref}}(\mu_0) &= \frac{L_{\text{ref}}(-\mu,\mu_0,\varphi-\varphi_0)}{R_{\text{ref}}(-\mu,\mu_0,\varphi-\varphi_0)} \\ &= \pi^{-1}E_{\text{dir}}(\mu_0) + \frac{\pi^{-1}}{R_{\text{ref}}(-\mu,\mu_0,\varphi-\varphi_0)} \\ &\quad \times \int_0^1\int_0^{2\pi} R_{\text{ref}}(-\mu,\mu',\varphi-\varphi')L_{\text{diff}}^{\text{inc}}(\mu',\mu_0,\varphi'-\varphi_0) \\ &\quad \times \mu'\,d\mu'\,d\varphi' \\ &\cong \pi^{-1}E_{\text{dir}}(\mu_0) + \pi^{-1}\int_0^1\int_0^{2\pi} L_{\text{diff}}^{\text{inc}}(\mu',\mu_0,\varphi'-\varphi_0)\mu'\,d\mu'\,d\varphi' \\ &= \pi^{-1}[E_{\text{dir}}(\mu_0) + E''_{\text{diff}}(\mu_0)] \end{aligned} \tag{21}$$

and R_{ref} is the known BRF of the reference target. Expressions (8), (20), and (21) then become the preferred algorithm equations instead of (3) and (4) for obtaining the highest accuracy in retrieved surface reflectance.

Multidirectional measurements of $L_{\text{diff}}^{\text{inc}}$ thus serve three major purposes: 1) They eliminate the need to know the atmospheric characteristics of the atmosphere; 2) they eliminate the sensitivity of the retrieved surface reflectances to instrument radiometric calibration uncertainties, when used in conjunction with reference target measurements; and (3) they eliminate the need to compute $L_{\text{diff}}^{\text{inc}}$ using complicated, time-consuming, multiple-scattering radiative-transfer routines. Measure-

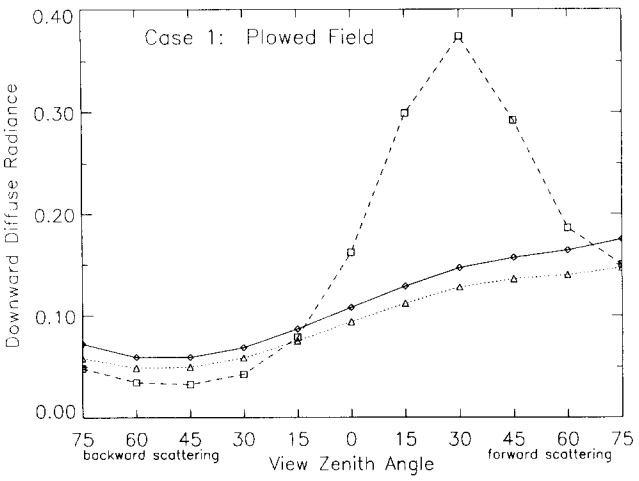

Figure 14. Incident diffuse radiance in the principal plane for BRF Case 1 (plowed field) and a solar zenith angle of 25.6°. The radiance is ratioed to the normal irradiance at the top of the atmosphere. The nominal aerosol model is shown (diamonds) in addition to the two variant models described in the text ($\omega = 0.9$, triangles; $g = 0.714$, squares).

ments of $L_{\text{diff}}^{\text{inc}}$ have an additional intrinsic accuracy in that they correctly account for the multiple reflections of radiation between the atmosphere and terrain surrounding the target without the need to assume that the terrain surface reflectance properties are the same as those of the target. This ability to bypass detailed knowledge of the atmosphere, the surrounding terrain, and the instrument calibration and still be able to perform an accurate surface BRF retrieval should be sufficient incentive for making multidirectional incident diffuse radiance measurements an integral part of surface BRF field work.

Once the surface BRF is accurately retrieved, it then is possible to analyze the incident diffuse radiation measurements with regard to retrieving aerosol optical properties. Figure 14 indicates that the dependence of diffuse radiance with view zenith angle is strongly dependent on the properties of the aerosols, particularly the phase function asymmetry, which, in turn, depends on the particle size distribution. For a solar zenith angle of 25.6°, the aerosol phase function which is more strongly forward scattering ($g = 0.714$) produces an aureole about the corresponding view zenith angle which is essentially absent from the other, less forward scattering, aerosol phase function ($g = 0.514$). Inversion techniques applied to aureole measurements for the retrieval of aerosol size distributions have been investigated previously (e.g., Green et al., 1971; Deepak, 1977; Nakajima et al., 1983). However, the analysis usually is limited to a relatively small angular range (about 20°) from the position of the sun where single scattering dominates. If the diffuse radiance measurements covering essentially the complete upward hemisphere are to be correctly analyzed, then the additional effects of multiple scattering, surface–atmosphere reflections, and finite instrumental field-of-view also must be adequately addressed.

A successful retrieval of the aerosol single scattering albedo using diffuse radiance measurements is highly dependent on the quality of the radiometric calibration of the instrument. A comparison of the diffuse radiance curves in Figure 14 with $\omega = 1.0$ and 0.9 shows basically a scaling difference between them, an effect which could easily be masked by instrumental calibration errors or uncetainties. When the aerosol optical depth is smaller than 0.5, the value illustrated in Figure 14, this difference becomes correspondingly smaller and more difficult to discern. Nevertheless, in spite of the problems in the interpretation of multidirectional downward diffuse radiance measurements, these data sets contain information about aerosol properties that is difficult to obtain otherwise.

SUMMARY

It is possible to retrieve accurate bidirectional reflectance factors using multidirectional measurements of surface reflected radiance provided that certain observational and measurement strategies are employed. Simulated ground level surface reflectance measurements, uniformly gridded in view angle over the whole downward-looking hemisphere, were used to show that the accuracy of the retrieved surface properties (bidirectional reflectance factors and directional hemispherical reflectance) was greatly improved if these gridded surface reflectance measurement sets were available over a wide range of solar zenith angles and were analyzed together in the retrieval algorithm. When a gridded set at a single sun position was analyzed separately, the accuracy of the resulting surface property retrieval was diminished to an extent depending on the aerosol optical depth and how sensitive the BRF was to the incident angle geometry; high sensitivity resulted in larger inaccuracies.

A rigorous retrieval algorithm involving iteration was described which preserved the full extent of the angular geometry of the surface BRF in the radiative transfer process and included all atmosphere–surface reflection effects. A relaxed version of the algorithm was also derived, having the virtues of speed and greater simplicity, but containing approximations which allowed the processing of gridded measurement sets at only a single solar zenith angle. It produced retrieval results which, in general, were less accurate than those from the rigorous algorithm when also processing only a single sun position measurement set. The technique of ratioing the surface reflectance measurements of a target with unknown surface properties to those from a refer-

ence target with ideal or near-ideal lambertian reflectance properties to obtain the bidirectional reflectance factor was shown to be essentially the same algorithm as the relaxed algorithm. The difference between them is that the relaxed algorithm must compute the direct irradiance and also the diffuse irradiance if the incident diffuse radiance is not measured, whereas the ratioing technique essentially measures them both.

This study found that a key measurement set, necessary for both accurate and efficient surface property retrievals, is that containing ground level multidirectional downward diffuse radiances, gridded over the upward-looking hemisphere in a similar fashion to the surface reflectance measurements. These measurements obviate the need for detailed knowledge of the atmospheric optical properties and the surrounding terrain reflection properties, both necessary inputs to the computation of downward diffuse radiances, and also the need to perform any detailed radiative transfer computations. In addition, if these gridded radiance measurement sets, both upward and downward directed, are complemented by reflectance measurements from a known, near-lambertian reference target, then the surface property retrievals are also insensitive to instrument radiometric calibration errors.

The author would like to express his appreciation to Eric Danielson for his assistance in the graphical aspects of this work and to the anonymous reviewers for their constructive comments. This research was carried out by the Jet Propulsion Laboratory, California Institute of Technology, under contract with the National Aeronautics and Space Administration.

REFERENCES

Charney, J., Quirk, W. J., Chow, S., and Kornfield, J. (1977), A comparative study of the effects of albedo change on drought in semi-arid regions, *J. Atmos. Sci.* 34:1366–1385.

Deepak, A. (1977), *Methods in Atmospheric Remote Sounding* (A. Deepak, Ed.), Academic, New York, pp. 265–295.

Deering, D. W., and Eck, T. F. (1987), Atmospheric optical depth effects on angular anisotropy of plant canopy reflectance, *Int. J. Remote Sensing*, 8:893–916.

Deering, D. W., and Leone, P. (1986), Sphere scanning radiometer for rapid directional measurements of sky and ground radiance, *Remote Sens. Environ.* 19:1–24.

Dickinson, R. E. (1981), Land surface processes and climate-surface albedos and energy balance, *Adv. Geophys.* 25: 305–353.

Dickinson, R. E., Pinty, B., and Verstraete, M. M. (1990), Relating surface albedos in GCM to remotely sensed data, *Agric. For. Meteorol.* 52:109–131.

Diner, D. J., Bruegge, C. J., Martonchik, J. V., et al. (1989), MISR: a Multi-angle Imaging SpectroRadiometer for geophysical and climatological research from EOS, *IEEE Trans. Geosci. Remote Sens.* GE-27:200–215.

Grant, I. P., and Hunt, G. E. (1968), Solution of radiative transfer problems using the invariant S_n Method, *Mon. Not. Roy. Astron. Soc.* 141:27–41.

Green, A. E. S., Deepak, A., and Lipofsky, B. J. (1971), Interpretation of the sun's aureole based on atmospheric aerosol models, *Appl. Opt.* 10:1263.

Irons, J. R., Ranson, K. J., Williams, D. L., Irish, R. R., and Huegel, F. G. (1991), An off-nadir pointing imaging spectroradiometer for terrestrial ecosystem studies, *IEEE Trans. Geosci. Remote Sens.* GE-29:66–74.

Kimes, D. S. (1983), Dynamics of directional reflectance factor distributions for vegetation canopies, *Appl. Opt.* 22:1364–1372.

Kimes, D. S., Newcomb, W. W., Nelson, R. F., and Schutt, J. B. (1985a), Directional reflectance distributions of a hardwood and pine forest canopy, *IEEE Trans. Geosci. Remote Sens.* GE-24:281–293.

Kimes, D. S., Newcomb, W. W., Tucker, C. J., et al. (1985b), Directional reflectance factor distributions for cover types of Northern Africa in NOAA 7/8 AVHRR Bands 1 and 2, *Remote Sens. Environ.* 18:1–19.

Markham, B. L., Halthorne, R. N., and Goetz, S. J. (1992), Surface reflectance retrieval from satellite and aircraft sensors: Results of sensor and algorithm comparisons during FIFE, *J. Geophys. Res.* 97(D17):18,785–18,795.

Martonchik, J. V., and Diner, D. J. (1992), Retrieval of aerosol optical properties from multi-angle satellite imagery, *IEEE Trans. Geosci. Remote Sens.* GE-30:223–230.

Martonchik, J. V., Danielson, E. D., Diner, D. J., and Bruegge, C. J. (1993), Retrieval of surface directional reflectance and hemispherical albedo using multi-angle measurements, in *IGARSS'93, Better Understanding of Earth Environment*, 18–21 August, Tokyo, Japan.

Mintz, Y. (1984), *The Global Climate* (J. T. Houghton, Ed.), Cambridge University Press, Cambridge, London, New York, pp. 79–105.

Nakajima, T., Tanaka, M., and Yamaguchi, T. (1983), Retrieval of the optical properties of aerosols from aureole and extinction data, *Appl. Opt.* 22:2951.

Nicodemus, F. E., Richmond, J. C., Hsia, J. J., Ginsberg, I. W., and Limperis, T. (1977), *Geometrical Considerations and Nomenclature for Reflectance*, NBS Monograph 160, National Bureau of Standards, U.S. Department of Commerce, Washington, DC.

Pinty, B., and Verstraete, M. M. (1991), Extracting information on surface properties from bidirectional reflectance measurements, *J. Geophys. Res.* 96:2865–2874.

Pinty, B., and Verstraete, M. M. (1992), On the design and validation of surface bidirectional reflectance and albedo models, *Remote Sens. Environ.* 41:155–167.

Starks, P. J., Norman, J. M., Blad, B. L., Walter-shea, E. A., and Walthall, C. L. (1991), Estimation of shortwave hemispherical reflectance (albedo) from bidirectionally reflected radiance data, *Remote Sens. Environ.* 38:123–134.